Available online at www.sciencedirect.com
ScienceDirect
International Journal of Heat and Mass Transfer 51 (2008) 1251–1263
International Journal of HEAT and MASS TRANSFER
www.elsevier.com/locate/ijhmt

Reynolds analogy in combustor modeling

Lei-Yong Jiang *, Ian Campbell

Gas Turbine Laboratory, Institute for Aerospace Research, National Research Council Canada, 1200 Montreal Road, M-10, Ottawa, Ontario, Canada K1A 0R6

Received 9 April 2007; received in revised form 31 October 2007
Available online 5 February 2008

Abstract

The Reynolds analogy concept has been used in almost all turbulent reacting flow RANS (Reynolds-averaged Navier–Stokes) simulations, where the turbulence scalar transfers in flow fields are calculated based on the modeled turbulence momentum transfer. This concept, applied to a diffusion flame model combustor, is assessed in this paper. Some of the numerical results, obtained from a flamelet combustion model with the turbulent Prandtl/Schmidt number varying from 0.25 to 0.85, are presented and compared with a benchmark experimental database. It is found that the turbulent Prandtl/Schmidt number has significant effects on the predicted temperature and species fields in the combustor. This is also true for the temperature profile along the combustor wall. In contrast, its effect on the velocity field is insignificant in the range considered. With an optimized turbulent Prandtl/Schmidt number, both velocity and scalar fields can be reasonably and quantitatively predicted. For the present configuration and operating conditions, the optimal Prandtl/Schmidt number is 0.5, lower than the traditionally used value of ~0.85. This study suggests that for accurate prediction of turbulence scalar transfers in practical reacting flows, the Reynolds analogy concept should be improved and new approaches should be developed.
Crown Copyright © 2007 Published by Elsevier Ltd. All rights reserved.

Keywords: Reynolds analogy; Turbulence scalar transfer; Combustor modeling; Schmidt number; Prandtl number

1. Introduction

Accurate prediction of temperature distribution is critical in the development of advanced combustion systems. For example, poor temperature profiles at the liner and exit of a gas turbine combustor can significantly reduce lifetime of the combustor and turbine vanes and blades behind. In extreme cases, devastating structural damage to engine components can occur.

In almost all turbulent reacting flow RANS simulations, turbulence scalar transfers (mixture fraction, species, and energy or temperature) are calculated based on the Reynolds analogy concept. In this approach, the turbulent Prandtl (Pr_t) and Schmidt (Sc_t) numbers are used to link the turbulence scalar transfers in flow fields to the momentum transfer that is determined by a selected turbulence model.

An existence of an analogy between the wall shear and heat flux in boundary layers was first postulated by Reynolds over a century ago [1]. This original hypothesis has been considerably amended and applied to general turbulent heat and species transfers [2,3]. Recently, its applications to high-Mach-number boundary layers [4], turbine flows [5] and film cooling [6] have been studied. The Reynolds analogy factors for flow parameters related to hypersonic propulsion and turbines have been determined [4,5].

The suitability of Reynolds analogy to disturbed turbulent thermal boundary flows has been reported by a number of authors. Choi and Orchard [7] investigated the heat transfer characteristics over a triangular-profiled riblet surface, while de Souza et al. [8] studied the large-scale organization of a boundary layer disturbed by a cylinder wake flow. They all pointed out that this concept did not hold in these disturbed boundary flows. Vogel and Eaton [9] carried out heat transfer and fluid dynamic measurements downstream of a backward-facing step. It was found that Reynolds analogy failed in the recovering boundary

* Corresponding author. Tel.: +613 993 9235; fax: +613 952 7677.
E-mail address: leiyong.jiang@nrc-cnrc.gc.ca (L.-Y. Jiang).

0017-9310/$ - see front matter Crown Copyright © 2007 Published by Elsevier Ltd. All rights reserved.
doi:10.1016/j.ijheatmasstransfer.2007.12.006

Nomenclature

C_p	specific heat at constant pressure
D	molecular diffusivity
f	mixture fraction
f''	fluctuating component of mixture fraction
H	total enthalpy
h	heat transfer coefficient
k	turbulence kinetic energy
Le	lewis number
M	molecular weight
p	probability density function
Pr_l	laminar Prandtl number
Pr_t	turbulent Prandtl number
r	radial coordinate
S	energy source term
Sc_t	turbulent Schmidt number
St	Stanton number
T	temperature
U	mean axial velocity
U_∞	free stream velocity
u	axial velocity component
$\mathbf{V}$	velocity vector
$\mathbf{v}''$	fluctuating velocity vector
v	radial velocity component
$u''v''$	turbulence shear stress, $\overline{\rho u'' v''}/\bar{\rho}$
x	coordinate along the combustor axis of symmetry
Y	species mass fraction
y^+	non-dimensional parameter, $\sqrt{\tau_w/\rho}y/\upsilon$
y	distance to the wall boundary
Z	mass fraction of element
Greek symbols	
Γ_t	turbulent Prandtl or Schmidt number
ε	turbulence dissipation rate
μ	laminar viscosity
μ_t	turbulent viscosity
ρ	density
τ_w	wall shear stress
υ	kinematic viscosity
ϕ	species mass fraction, mixture fraction, or total enthalpy
ϕ''	scalar fluctuation component
φ	species mass fraction, density or temperature
ω	species source term

layer, and it was only valid far downstream of the reattachment point. Time-resolved gas temperature in the oscillating turbulent flow of a pulse combustor tail pipe was studied by John and Keller [10]. The results indicated that the analogy between momentum and thermal transport at the tail pipe wall was no longer valid.

Since the 1970s, the Reynolds analogy concept has been further extended into computational simulations of general turbulent reacting or mixing flows. The main advantage of this approach is that the turbulence scalar transfers can be effectively computed from the modeled momentum transfer without solving a full second moment closure for both momentum and scalar transportations. Consequently, the computing time to reach a converged solution is much reduced.

Numerous experimental studies on Pr_t and Sc_t were carried out in the last century, particularly in the period of 1930s–1970s [2,3]. Hinze [2] reviewed a large number of experimental measurements in pipe and 2D channel flows, and pointed out that the overall Pr_t or Sc_t varied from 0.6 to 0.8. Recently, based on their velocity and concentration half-width measurements in axisymmetric jets of air and helium, Panchapakesan and Lumley [12] obtained an average value of 0.7 for Sc_t.

In most turbulent reacting or mixing flow simulations, it has become a common practice to set $Le \equiv Sc_t/Pr_t = 1$ or $Pr_t = Sc_t$ [11]. Traditionally a constant value of $Pr_t = Sc_t \approx 0.85$ has been used in jet flows [13,14] and gas turbine combustor modeling [15,16]. However, low Pr_t and Sc_t numbers from 0.20 to 0.5 have been used by a number of authors for simulating kerosene-fired gas turbine combustors. Crocker et al. [17] successfully modeled an entire combustor from the compressor diffuser exit to the turbine inlet, including air split and liner wall temperature prediction. A low value of 0.25 was used for Pr_t and Sc_t since it consistently demonstrated better agreement with the combustor fuel/air mixing results. Kaaling et al. [18] systematically studied five RQL (rich burn, quick quench, lean burn) low-emission combustor designs. The CFD calculations were calibrated against CARS (coherent anti-Stokes Raman spectroscopy) temperature measurements, and good agreement was found by using $Pr_t = Sc_t = 0.2$. Large eddy simulations (LES) of a Rolls–Royce production gas turbine combustor were performed by Cannon et al. [19], where $Pr_t = Sc_t = 0.5$. Moreover, the effect of Schmidt number on turbulence scalar mixing of a gaseous jet issued into a cross airflow was investigated by He et al. [20]. By comparison with the available experimental data, $Pr_t = Sc_t = 0.2$ was recommended.

To provide a benchmark database for the evaluation and development of various physical models, a series of experiments were performed on a diffusion flame model combustor at the National Research Council of Canada (NRCC). The comprehensive results include mean and fluctuating velocity components, mean temperature, wall temperature, radiation heat flux, as well as species concentrations [21].

The objectives of the present work are to find out if such a low value of Pr_t and Sc_t is a real physical fact in combustor modeling, and to assess the Reynolds analogy concept

currently used in turbulent reacting flow RANS simulations. Since the model combustor geometry is much simpler than practical combustors, its boundary conditions are well defined and a comprehensive experimental database is available, the assessment of the above issues is relevant.

2. Experimental measurements

A schematic diagram of the model combustor is shown on the left side of Fig. 1, including the fuel and air inlets, combustion chamber and contracted exhaust section (all dimensions are in mm). Air entered the combustion chamber around a disc flame-holder, while fuel was fed through the center of the bluff body. The test rig was mounted on a three-axis traversing unit with an accuracy of ±100 μm. Fuel used in the experiments was commercial grade propane, and dry air was delivered from a shop air supply. Both air and fuel flows were controlled by Sierra side-trak mass-flow controllers with 2% accuracy of full scale (fuel 100 l/min and air 2550 l/min).

To reduce the heat losses through walls, a 25.4 mm thick fibre blanket of Al_2O_3 was wrapped around the combustion chamber. Four narrow slots were cut into the blanket to allow appropriate physical and optical access to the chamber interior. Interchangeable sets of stainless steel and fused silica windows were used, the former for physical probing with gas sampling probes, radiometers and thermocouples, and the latter for optical probing with a laser Doppler anemometer (LDA). The viewing area of the windows measured 17 mm in width and 344 mm in length.

Measurements of velocity were made using both a two- and three-component LDA system operating in a back scattering mode. In the lower section of the combustion chamber, limited optical access forced the use of a single fibre optic head to measure axial and tangential velocities. In the upper section of the chamber, a complete three-component LDA system was used. Gas temperatures were acquired using an uncoated 250 μm diameter, type "*S*" thermocouple supported by a twin-bore ceramic tube. Thermocouples embedded in and flush with the combustor wall were used to measure the wall temperature. Gas species measurements were made with a sampling probe connected to a Varian Model 3400 Gas Chromatograph. The major species measured were CO, CO_2, H_2O and C_3H_8.

3. Numerical simulations

Axisymmetric, steady, turbulent, reacting flows were considered in the present study, and a commercial software package, fluent, was used as the platform for all numerical simulations. The computational domain, governing equations, selected physical models, boundary conditions and solution methods are described in the following subsections.

3.1. Computational domain

The computational domain covered the entire combustor flow field from the fuel and air inlets to the exhaust exit, as shown on the right side of Fig. 1. The internal and external conjugate heat transfers from the combustion mixture to the flame-holder body and insulation walls were also modeled.

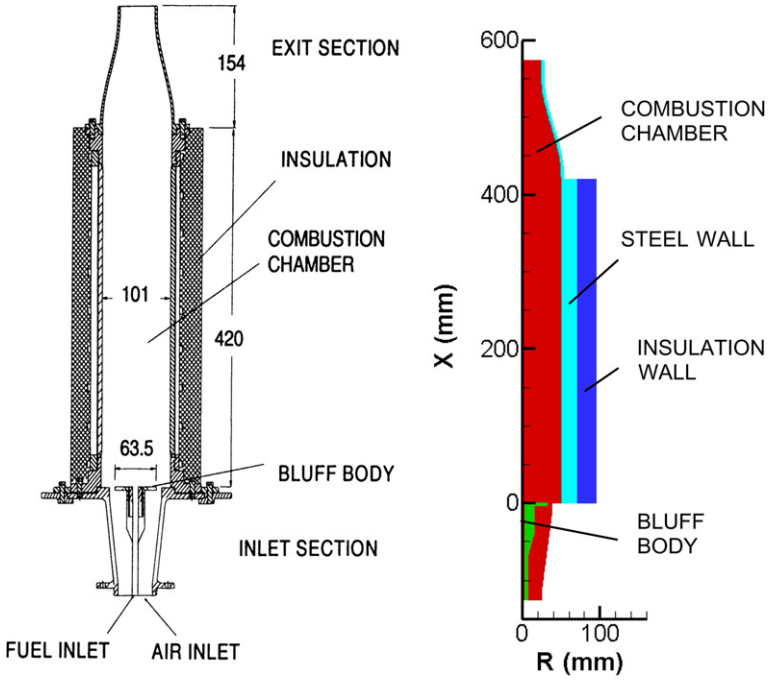

Fig. 1. The model combustor and computational domain.

Since the flow field was axisymmetric, 2D quadrilateral meshes were used. Fine grids were laid behind the flame-holder in the combustion chamber in order to resolve the recirculation region. Fine grids were also generated in the shear layers between the recirculation region and fuel and air jets, as well as in the gap between the flame-holder edge and air inlet chamber wall. Coarse grids were used in the stainless steel walls and ceramic blanket. A total of 74,100 elements was used for most of the simulations. The skewness was less than 0.2 in the flow field domain and the aspect ratio was less than 12 for 99.5% elements. Efforts were made to keep the wall parameter, y^+ ($\sqrt{\tau_w/\rho}y/\upsilon$), in the desired range (30–60). A number of meshes were tested to ensure mesh independence of the numerical results.

3.2. Governing equations

The first-moment Favre-averaged conservation equations for mass, momentum, species, mixture fraction and total enthalpy, may be expressed in a coordinate-free form as [22,23]

$$\nabla\cdot\left(\bar{\rho}\widetilde{\mathbf{V}}\right)=0 \tag{1}$$

$$\nabla\cdot\left(\bar{\rho}\widetilde{\mathbf{V}}\widetilde{\mathbf{V}}\right)=-\nabla\bar{p}+\nabla\cdot\mathbf{T}-\nabla\cdot\left(\overline{\rho\mathbf{v}''\mathbf{v}''}\right) \tag{2}$$

$$\nabla\cdot\left(\bar{\rho}\widetilde{\mathbf{V}}\widetilde{Y}_i\right)=\nabla\cdot\left(\rho D_i\nabla\widetilde{Y}_i\right)-\nabla\cdot\left(\overline{\rho\mathbf{v}''Y_i''}\right)+\omega_i \tag{3}$$

$$\nabla\cdot\left(\bar{\rho}\widetilde{\mathbf{V}}\tilde{f}\right)=\nabla\cdot\left(\rho D\nabla\tilde{f}\right)-\nabla\cdot\left(\overline{\rho\mathbf{v}''f''}\right) \tag{4}$$

$$\nabla\cdot\left(\bar{\rho}\widetilde{\mathbf{V}}\widetilde{H}\right)=\nabla\cdot\left(\frac{\mu}{Pr_l}\nabla\widetilde{H}\right)-\nabla\cdot\left(\overline{\rho\mathbf{v}''H''}\right)+S_H \tag{5}$$

In the above equations, $\bar{\rho}$ represents mean density, $\widetilde{\mathbf{V}}$ is the mean velocity vector, $\mathbf{v}''$ stands for fluctuation velocity vector, the viscous stress tensor $\mathbf{T}=\mu[\nabla\widetilde{\mathbf{V}}+(\nabla\widetilde{\mathbf{V}})^{\mathrm{T}}]-\frac{2}{3}\mu\nabla\cdot\widetilde{\mathbf{V}}\mathbf{I}$ with $\mathbf{I}$ a unit tensor, $\overline{\rho\mathbf{v}''v''}$ denotes Reynolds stresses, Y_i is the mass fraction of the ith species, f stands for mixture fraction, H denotes total enthalpy, and D and Pr_l represent molecular diffusivity and Prandtl number, respectively.

For closure of the above equations, the species source term, ω_i in Eq. (3) is obtained from a selected combustion model. The energy source term, S_H in Eq. (5) includes viscous heating and radiation heat transfer that is obtained from a radiation model. As mentioned earlier, Reynolds stresses, $\overline{\rho\mathbf{v}''v''}$ or turbulence momentum transfer in Eq. (2) are modeled by a selected turbulence model, while $\overline{\rho\mathbf{v}''Y''}$, $\overline{\rho\mathbf{v}''f''}$, $\overline{\rho\mathbf{v}''H''}$ or turbulence scalar transfers in Eqs. (3)–(5) are computed based on Reynolds analogy.

3.3. Turbulence modeling and Reynolds analogy

In a previous benchmarking on turbulence modeling [24], the Reynolds stress model (RSM) produced better results than three popular two-equation eddy-viscosity models. Therefore, it was chosen to model turbulence momentum transfer in the present flow. Since detailed description of the RSM takes a lot of space and is beyond the scope of the present paper, it is not given here. It can be readily found in Refs. [23,25].

For axisymmetric flows, as in the present case, only four Reynolds stress components need to be considered. The four transportation equations of these components along with the turbulence dissipation rate equation are solved in the combustor flow field. From the solutions of Reynolds stresses and dissipation rate, the turbulent viscosity (momentum transfer coefficient) is then computed:

$$\mu_t=\bar{\rho}C_\mu k^2/\varepsilon \tag{6}$$

where $C_\mu=0.09$, and k and ε are turbulent kinetic energy and dissipation rate, respectively.

Following the Reynolds analogy concept, the turbulence scalar transfers are modeled as

$$-\nabla\cdot\overline{\rho\mathbf{v}''\phi''}\cong\nabla\cdot\left(\frac{\mu_t}{\Gamma_t}\nabla\tilde{\phi}\right) \tag{7}$$

where ϕ stands for species mass fraction, mixture fraction or total enthalpy, and Γ_t represents Pr_t or Sc_t. Note that in Eq. (7), the turbulence scalar transfer coefficients, μ_t/Γ_t, are simply the products of the turbulence momentum transfer coefficient (μ_t) and $1/\Gamma_t$. The isotropic turbulence transfer (coefficient) assumption is abandoned in momentum transfer; however, it is still used for turbulence scalar transfers.

The rationale and limitation of Reynolds analogy could be revealed by reducing the conservation Eqs. (2)–(5) to axisymmetric steady boundary flows and neglecting the streamwise pressure gradient, molecular viscous terms, and source terms. Then the following equations are obtained:

$$\bar{\rho}\tilde{u}\frac{\partial\tilde{u}}{\partial x}+\bar{\rho}\tilde{v}\frac{\partial\tilde{u}}{\partial r}=\frac{1}{r}\frac{\partial}{\partial r}\left(r\mu_t\frac{\partial\tilde{u}}{\partial r}\right) \tag{8}$$

$$\bar{\rho}\tilde{u}\frac{\partial\tilde{\phi}}{\partial x}+\bar{\rho}\tilde{v}\frac{\partial\tilde{\phi}}{\partial r}=\frac{1}{r}\frac{\partial}{\partial r}\left(r\frac{\mu_t}{\Gamma_t}\frac{\partial\tilde{\phi}}{\partial r}\right) \tag{9}$$

where the turbulent viscosity concept is applied to both streamwise momentum and scalar transfers. With $\Gamma_t=1$, the two-equations become identical. That is, under appropriate boundary conditions, the solution of all these flow parameters can be obtained from a single partial differential equation [11]. For wall boundary flows with relatively large radius with respect to boundary thickness, the original form of Reynolds analogy can be deduced [5]:

$$\frac{2St}{c_f}=\frac{(h/\rho C_p U_\infty)}{(\tau_w/\rho U_\infty^2)}\approx 1 \tag{10}$$

where $St=h/(\rho C_p U_\infty)$ is the Stanton number and $c_f=\tau_w/(0.5\rho U_\infty^2)$ is the wall friction coefficient. From this equation, the turbulent heat transfer coefficient can be estimated from the measurement of pressure loss due to friction in the flow.

3.4. Combustion modeling

Some of the numerical solutions obtained from a laminar flamelet combustion model are presented and discussed in this paper. The laminar flamelet model views the turbulent flame as an ensemble of laminar flamelets [26]. For diffusion flames, it approximates the unsteady distorted turbulent diffusion flame using a steady laminar counter-flow diffusion flame.

The governing equations for laminar counter-flow diffusion flames can be transformed from physical coordinates to a mixture fraction coordinate by neglecting some insignificant terms. In the adiabatic case, the species fractions, density and temperature along the flamelet axis (normal to the flamelet) can be uniquely determined by two parameters, the mixture fraction, f, and the scalar dissipation rate, χ_{st}, at the position where f is stoichiometric.

The mixture fraction can be written as

$$f = \frac{Z_i - Z_{i,ox}}{Z_{i,fuel} - Z_{i,ox}} \tag{11}$$

where Z_i stands for the mass fraction of element, "i", $Z_{i,ox}$ and $Z_{i,fuel}$ denote the elemental mass fraction of "i" at the oxidizer and fuel inlets, respectively. The scalar dissipation rate in turbulent flows is modeled by the following expression:

$$\chi_{st} = C_\chi \varepsilon \overline{f''^2}/k \tag{12}$$

where $C_\chi = 2.0$. The coupling between non-equilibrium chemistry and turbulence is accounted for by the β-function probability density function, and the time-averaged flow parameters in the non-adiabatic condition are computed from the following equation:

$$\overline{\varphi_i} = \int_0^1 p\left(\tilde{f}, \overline{f''^2}\right) \varphi_i(f, \chi_{st}, H) \mathrm{d}f \tag{13}$$

where φ represents species mass fraction, density or temperature, and H is the total enthalpy. The flamelet library can be pre-processed and tabulated, which offers tremendous computational saving.

It should be mentioned that fluctuation of the scalar dissipation rate in Eq. (13) is ignored, which has become a common practice [27]. A number of approaches have been proposed to account for fluctuation of the scalar dissipation rate [26]; however, there is no conclusive solution. Moreover, it may be argued that the turbulence effect on the scalar dissipation rate could have been, to some extent, modeled by Eq. (12) and the probability density function of the mixture fraction in Eq. (13). In short, this is still an open area of research.

A major advantage of the flamelet model over other combustion models, such as eddy-dissipation and probability density function models, is that detailed and more realistic chemical kinetics can be incorporated into turbulent reacting flows. In the present study, the chemical reaction mechanism from Stahl and Warnatz [28] for propane–air flames was employed. It consists of 228 chemical reactions and 31 species, including O, O_2, OH, H, H_2, H_2O, H_2O_2, HO_2, N_2, CO, CO_2, CH, CH_2, CH_3, CH_4, CHO, CH_2O, CH_2CO, CH_3CO, CH_3CHO, C_2H, C_2H_2, C_2H_3, C_2H_4, C_2H_5, C_2H_6, C_3H_6, C_3H_8, $N^*C_3H_7$, $I^*C_3H_7$ and C_2HO.

3.5. Other physical models

To account for the radiation heat transfer between the gas mixture and the combustion chamber walls, a discrete ordinates radiation model [29] was employed. The absorption coefficient of the gaseous mixture was determined from local species mass fractions in the flow. An absorption coefficient of 0.5 was used for the stainless steel wall and the disc flame-holder. For internal wall boundaries, as mentioned earlier, effort was made to keep the y^+ value in the desired range of 30–60. However, there were local regions where y^+ value was outside this range. To minimise this effect, an enhanced wall boundary treatment was applied at all internal walls. In this approach, a two-layer model is combined with wall functions, and the viscous and fully turbulent regions are smoothly blended.

Polynomials determined from the JANAF tables [30] were used to calculate the specific heat of each species as a function of temperature. For other thermal properties of the mixture such as molecular viscosity and thermal conductivity, the values of air at 900 K were used. The thermal conductivity was 25 W/m K for the stainless steel, and 0.1 W/m K for the ceramic insulation.

3.6. Boundary conditions

The fuel mass-flow rate was 16.2 g/s and the airflow rate was 550 g/s, and the corresponding overall equivalence ratio was 0.46. For both flows, the inlet temperature was 293 K. The Reynolds number based on the air entry velocity and flame-holder diameter was 1.9×10^5. An estimated turbulence intensity of 10% and hydraulic diameters were used to estimate Reynolds stress components and turbulence dissipation rate at the fuel and air inlets. A sensitivity study was performed with the inlet turbulence intensity of 5% and 2%, respectively. The difference in computed turbulence kinetic energy along the combustor centerline is observable only in the fuel inlet passage and a small region near $x = 80$ mm, and the maximum deviation between case 2% and case 10% is only 2.3%. The difference is even smaller for the mean axial velocity and temperature along the combustor centerline.

The external wall temperatures were defined based on the experimental measurements. A room temperature of 293 K was assigned to the walls of the inlet section, and the upstream edges of the combustion chamber and ceramic insulation walls. A linear temperature profile from 294 to 405 K was specified along the outer boundary of the ceramic insulation wall. The temperature of the outer boundary of the exit section was set to 960 K. The same temperature was assigned to the downstream edge of the combustion chamber wall because its heat resistance was

much smaller than the ceramic insulation. A linear temperature profile from 960 to 405 K was assigned to the downstream edge of the insulation wall. Finally, the pressure at the combustor exit was set to the atmospheric value.

3.7. Solution methods

A segregated solver with a second-order accurate scheme was used to resolve the flow field. A node-based method for derivatives was chosen in order to maintain numerical stability as Γ_t approached 0.25. At convergence, the normalized residuals of flow variables were less or equal to 10^{-5} in all test cases. The monitored axial velocities at two points in the shear layer downstream of the flame-holder remained unchanged at least for the first four digits. A 4-node LINUX cluster, 64-bit, 2.6 GHz, dual CPU and 8 GB RAM for each node, was used to perform all simulations.

4. Results and discussion

Numerical simulations were performed with Γ_t varying from 0.25 to 0.85, and a large amount of data were processed and analyzed. As stated earlier, only some of the results are presented here. In the following sub-sections, the velocity field results are first presented, then the temperature and species results are discussed, and finally the Reynolds analog concept is assessed.

4.1. Velocity distributions

The upper half of Fig. 2 shows the axial velocity contours and flow path-lines for $\Gamma_t = 0.85$. The lower half of the figure presents the experimental data with the zero axial velocity lines specified. The flow patterns in the combustion chamber are excellently predicted. Two recirculation zones are formed behind the flame-holder although, in the experimental case, the central recirculation zone is not completely resolved and no flow path-lines are drawn due to the limited data points. It is significant that both reattachment points or lengths of the two recirculation zones are well predicted. The central recirculation zone created by the fuel jet is completely confined within the annular recirculation zone generated by the annular air jet. This implies that the transportation of fuel into the flow field is realized by laminar and turbulent diffusion only through the annular recirculation zone.

Although turbulence scalar transfers are calculated based on the modeled turbulence momentum transfer, the former also affects the latter since they are coupled. The effect of Γ_t on velocity field is illustrated in Figs. 3 and 4 for $\Gamma_t = 0.50$ and 0.25, respectively. The differences in the flow fields between $\Gamma_t = 0.85$ and 0.50 are minor. For $\Gamma_t = 0.25$, the length and volume of the annular recirculation zone are slightly reduced in comparison with those in Figs. 2 and 3. The numerical results indicate that in the range of Γ_t studied, the effect of Γ_t on velocity field is limited, particularly for $\Gamma_t > 0.35$.

Fig. 5 gives axial velocity profiles along the combustor centerline, and compares the results with the experimental measurements. Superimposed in the figure, in red, are the estimated error bars of 2%. The numerical results show good agreement with the experimental data, except that the peak value of negative velocity is under-predicted. The effect of Γ_t variation from 0.85 to 0.25 on the centerline velocity profile is small.

The predicted axial velocity profiles at five cross-sections, two inside the recirculation region, one close to the stagnation point, and the last two located downstream of the recirculation region, are presented in Fig. 6, and quantitatively compared with the experimental results. In general, the profiles are reasonably predicted except in the local regions at three middle sections, where the discrepancies increase as Γ_t decreases. At these three sections, the flow field is complex, which represents a difficult task for numerical simulations.

Fig. 7 shows quantitative comparisons of turbulence kinetic energy between the numerical and experimental results at four cross-sections from $x = 60$ to 240 mm. In the figure, error bars show the measurement accuracy of ±8%. The trends and magnitudes are reasonably well predicted, except for the magnitudes at three downstream sections with $\Gamma_t = 0.25$.

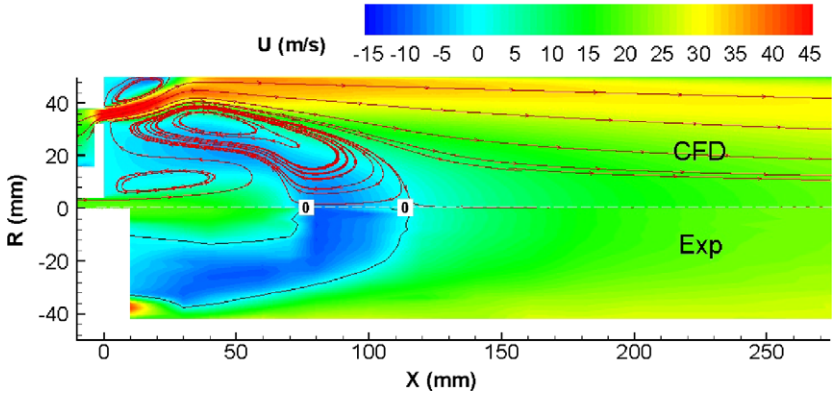

Fig. 2. Axial velocity contours and flow path-lines, $\Gamma_t = 0.85$.

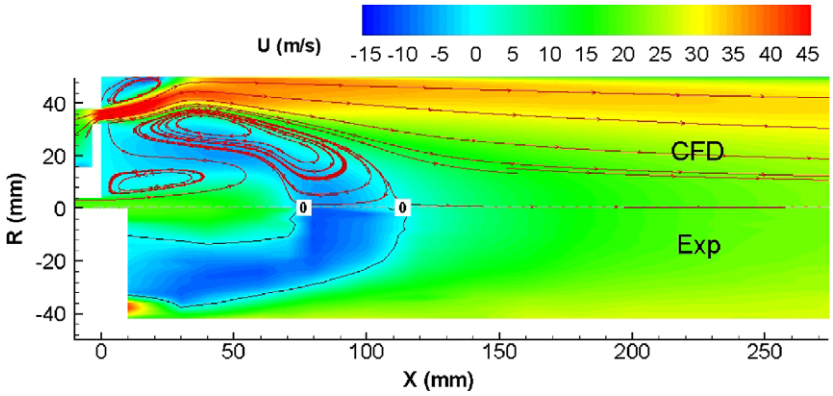

Fig. 3. Axial velocity contours and flow path-lines, $\Gamma_t = 0.50$.

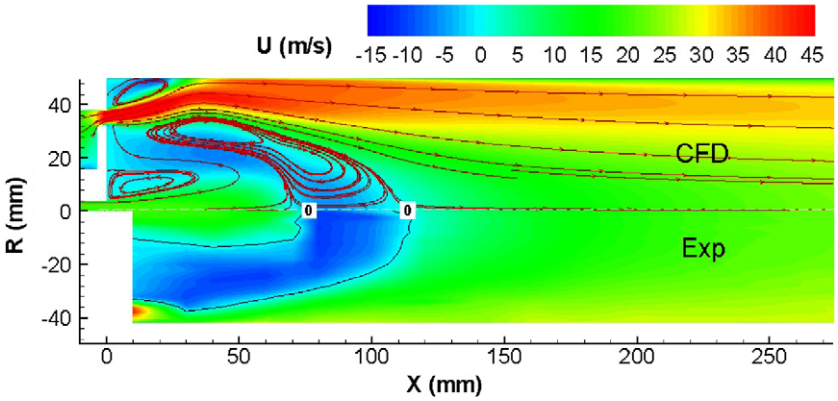

Fig. 4. Axial velocity contours and flow path-lines, $\Gamma_t = 0.25$.

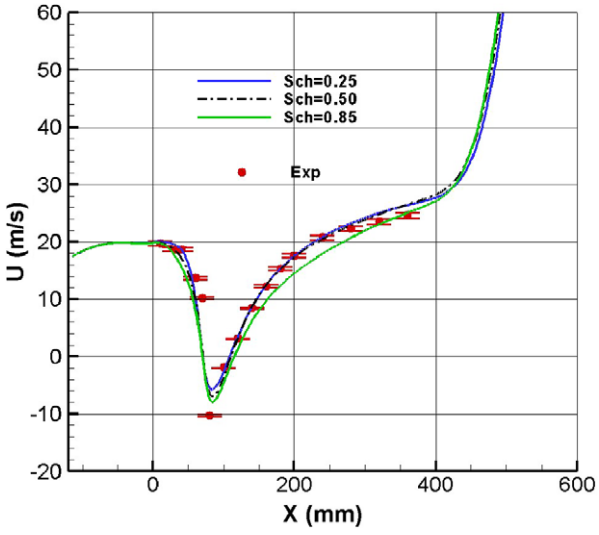

Fig. 5. Axial velocity profiles along the combustor centerline.

Fig. 8 compares the numerical results of turbulence shear stress, $\overline{\rho u'' v''}/\bar{\rho}$ with the measured experimental data at four cross-sections. Here the estimated measurement accuracy is about 12%. The shear stress is of primary interest for momentum transport in turbulent flows, particularly in shear flows. Again, the trends and magnitudes are reasonably well predicted at all sections. The effect of Γ_t variation is insignificant, particularly in comparison with the measurement error.

The above numerical results indicate that the effect of Γ_t variation on the predicted velocity field is limited, and the velocity fields predicted by the RSM turbulence model agree reasonably well with the experimental data for $\Gamma_t > 0.4$. Proper prediction of velocity fields (or momentum transfer) is a prerequisite for adequate evaluation of Reynolds analogy or Γ_t effect on the temperature field of turbulent reacting flows. This is because the turbulence scalar transfers (and then the temperature field) in the flow are obtained from the modeled momentum transfer using Reynolds analogy. Based on the acceptable velocity fields, the Reynolds analogy concept is assessed.

4.2. Temperature distributions

The temperature contours for $\Gamma_t = 0.85$, 0.5 and 0.25 are presented and compared with the experimental database in Figs. 9–11, respectively. As expected, the temperature in the recirculation region is relatively uniform due to strong turbulent mixing. Intense chemical reaction takes place around the envelope of the annular recirculation zone. In comparison with the experimental data, the high temperature region is shifted downstream for $\Gamma_t = 0.85$,

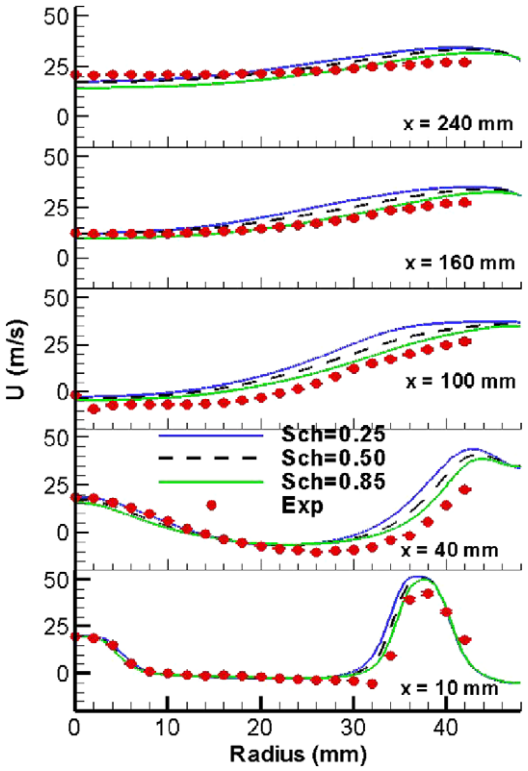

Fig. 6. Axial velocity profiles at sections, $x = 10$–240 mm.

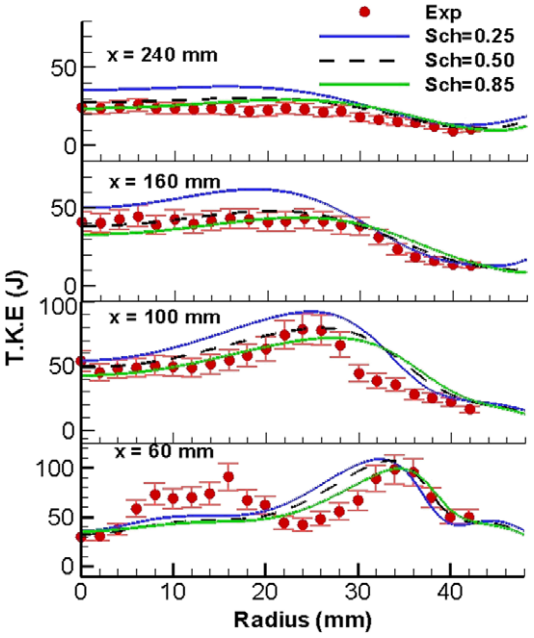

Fig. 7. Turbulence kinetic energy profiles at sections, $x = 60$–240 mm.

significantly reduced and shifted upstream for $\Gamma_t = 0.25$, and best predicted with $\Gamma_t = 0.50$. In short, the high temperature region moves upstream and becomes smaller with decreasing Γ_t. This is because the turbulence transfer of fuel into the airflow and then the chemical reaction are accelerated as Γ_t decreases.

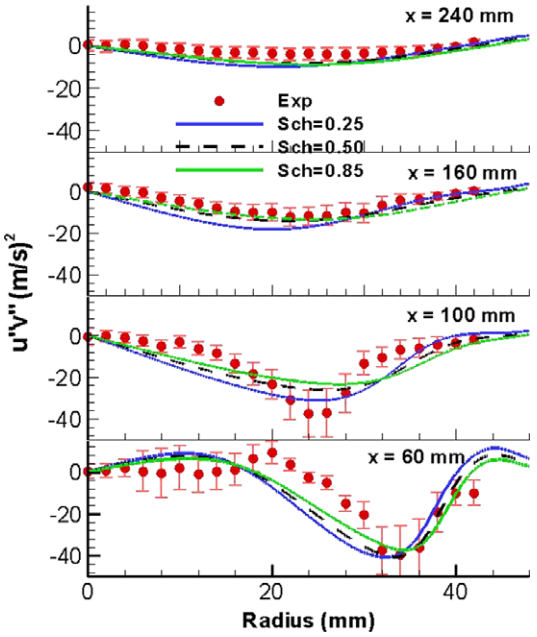

Fig. 8. Turbulence shear stress profiles at sections $x = 60$–240 mm.

In Figs. 9–11, it is found that the predicted temperature in the high temperature region is higher than the measured values. The maximum difference is about 170 K. The main reason may be that the temperature was measured by a 0.25 mm diameter thermocouple, as mentioned earlier. Owing to the radiation and conduction losses from the thermocouple, the measurement error could exceed 100 K over regions where the gas temperature was high and the flow velocity was low [31].

The effect of Γ_t on the predicted flame length is illustrated in Fig. 12. The flame region is represented by the stoichiometric line of the mean mixture fraction ($\tilde{f} = 0.0603$) in the upper of the figure, and by the OH mole-fraction contour lines in the lower half. The effect of Γ_t on the flame length and region is obvious. As Γ_t decreases from 0.85 to 0.25, both the flame length and region are significantly reduced, and the flame length decreases about three times from 342 to 110 mm.

The predicted temperature profiles along the combustor centerline are compared with the experimental data in Fig. 13, where the measurement error is about 5%. In the upstream region ($x < \sim 80$ mm), the effect of Γ_t is limited; the numerical results for $\Gamma_t = 0.50$ and 0.85 agree well with the experimental data. In contrast, the effect of Γ_t is apparent in the downstream region. It is because in the upstream region the fuel distribution or chemical reaction is mainly determined by the location and size of the annular recirculation zone, which is formed by complex flow interactions among the central fuel jet, annular airflow and two recirculation zones. That is, the flow is convection-dominated. However, in the downstream region, the turbulent diffusion or transfer plays a dominant role in the fuel spreading away from the axis of symmetry, where the flow path-lines are almost parallel to each other as shown in Figs. 2–4. In

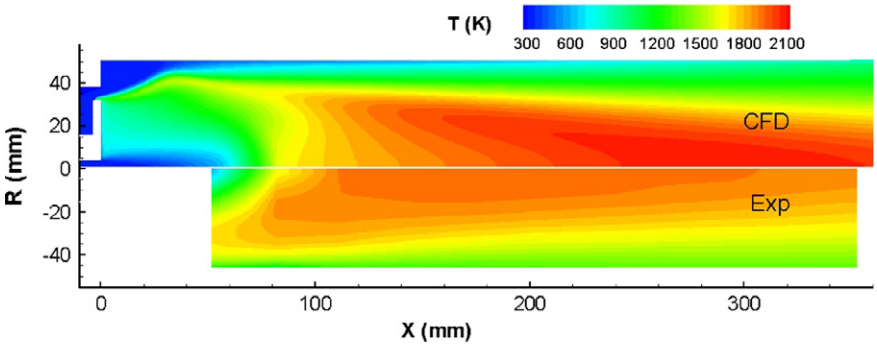

Fig. 9. Temperature contours, $\Gamma_t = 0.85$.

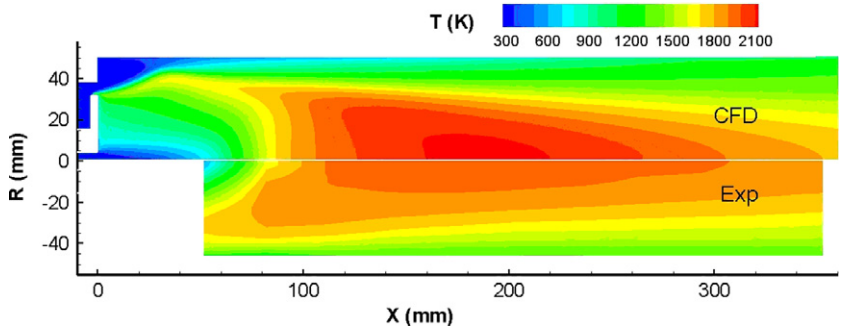

Fig. 10. Temperature contours, $\Gamma_t = 0.50$.

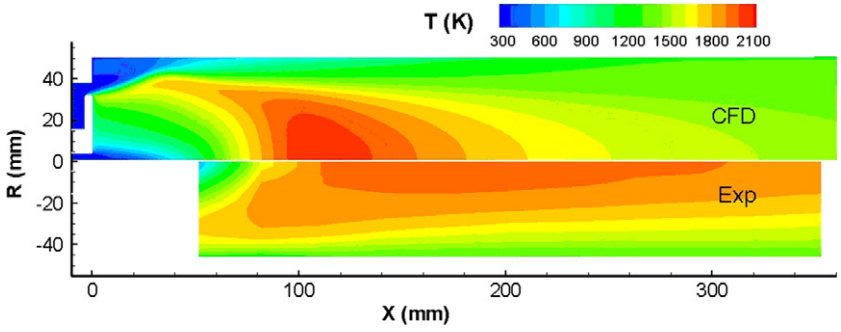

Fig. 11. Temperature contours, $\Gamma_t = 0.25$.

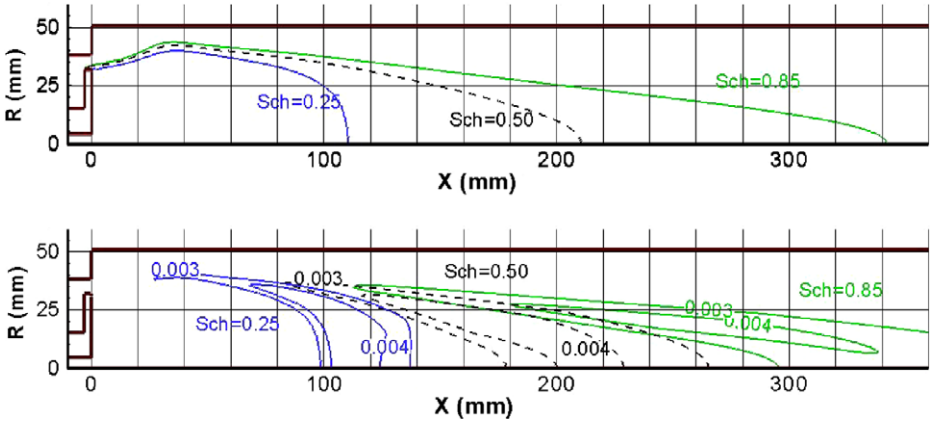

Fig. 12. Variation of predicted flame length with Γ_t.

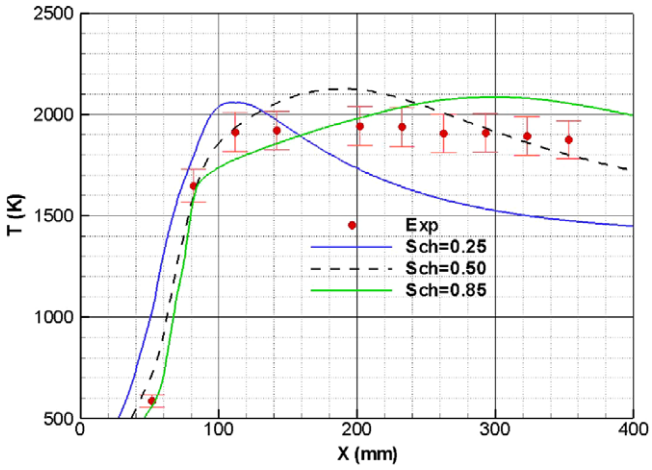

Fig. 13. Temperature profiles along the combustor centerline.

Fig. 13, $\Gamma_t = 0.50$ gives the best results although the predicted profile shows a peak in the middle portion, while the measurements tend to be flat. The predicted maximum temperature reaches 2120 K, while the measured value is 1950 K.

Fig. 14 presents the temperature profiles for $\Gamma_t = 0.85$, 0.50 and 0.25 at five cross-sections, $x = 52$–233 mm. As expected, at all sections, with Γ_t decreasing the temperature profiles become flatter, i.e., the fuel spreading becomes faster. The numerical results from $\Gamma_t = 0.50$ agree reasonably well with the experimental results, except for the regions near the combustor wall. In these near-wall regions, the temperature is under-predicted, which may suggest that the fuel spreading is under-predicted in these local regions.

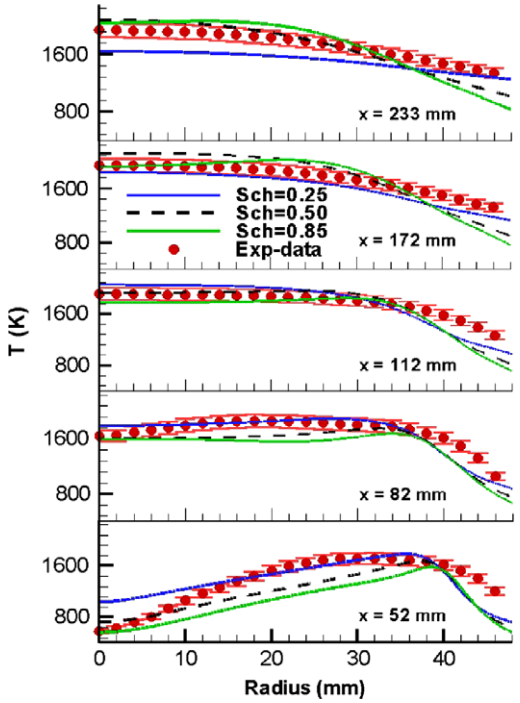

Fig. 14. Temperature profiles at sections $x = 52$–233 mm.

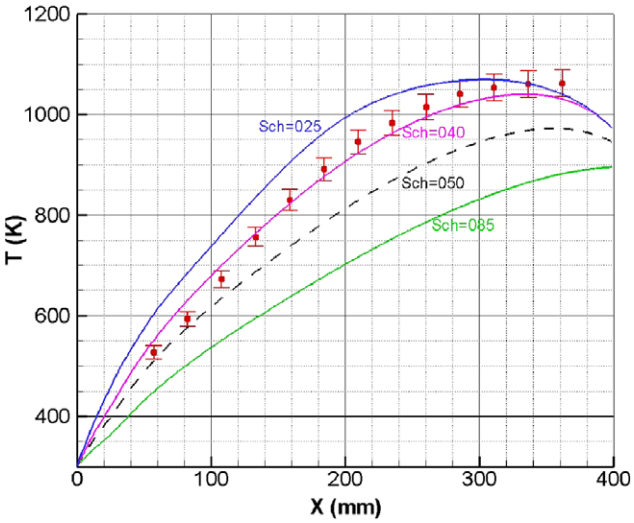

Fig. 15. Temperature profiles along the combustor wall.

Poor performance is observed for $\Gamma_t = 0.25$ at $x = 52$ and 233 mm, and $\Gamma_t = 0.85$ at $x = 52$ mm. A strong effect of Γ_t is observed at all sections.

Variation of combustor wall temperature with Γ_t is shown in Fig. 15. The numerical results are compared with the experimental data that have a measurement error of ~2.5%. Unsurprisingly, the predicted wall temperature increases as Γ_t decreases. The results of $\Gamma_t = 0.40$ show best agreement with the measurements, although the wall temperature is slightly over-predicted in the upstream region and under-predicted in the downstream region. As noticed, this Γ_t value does not agree with the preferred value of 0.50 for the temperature prediction inside the combustor. This may suggest that varying Γ_t, instead of a constant value, should be used in turbulent reacting flow simulations.

4.3. Species distributions

Water is one of the major products in propane–air combustion. Fig. 16 presents the H_2O mole-fraction profiles at six sections and the results are compared with the experimental data (which have a 5% measurement error). To illustrate the main features of chemical reactions, the locations of the six sections are selected as, one across the central recirculation zone, another passing through both recirculation zones, the third cutting through the annular recirculation zone, the fourth almost passing through the stagnation point, and then followed by two downstream sections (see Figs. 2–4).

The H_2O profile becomes flatter as Γ_t decreases, particularly for downstream sections, which is consistent with the trends observed for the temperature profiles in Fig. 14. Stronger effects of Γ_t are found at downstream sections, $x > 112$ mm, as well as in the central region at the upstream section, $x = 52$ mm. The results for $\Gamma_t = 0.50$ and 0.85 are close to each other, and $\Gamma_t = 0.50$ gives the best agreement with the experimental data at most sections. The numerical results with $\Gamma_t = 0.25$ show large deviations from the

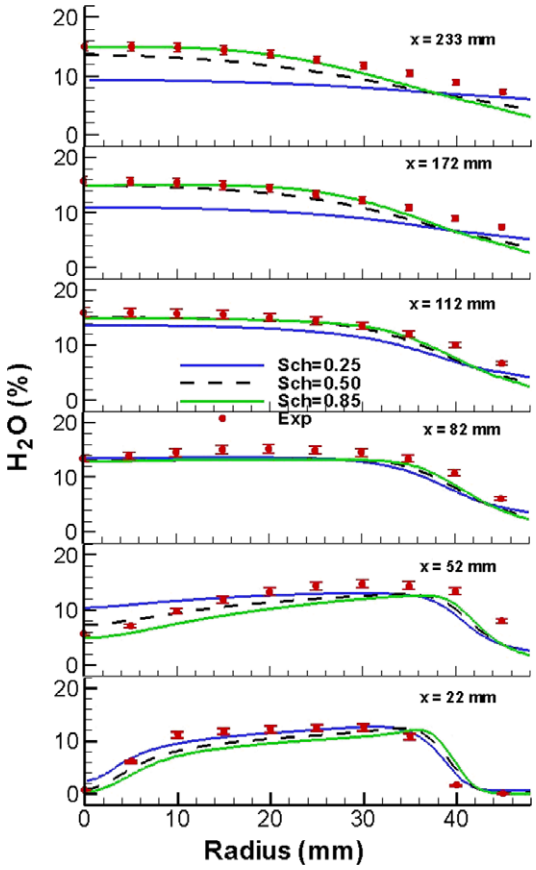

Fig. 16. H_2O profiles at cross-sections, $x = 22$–233 mm.

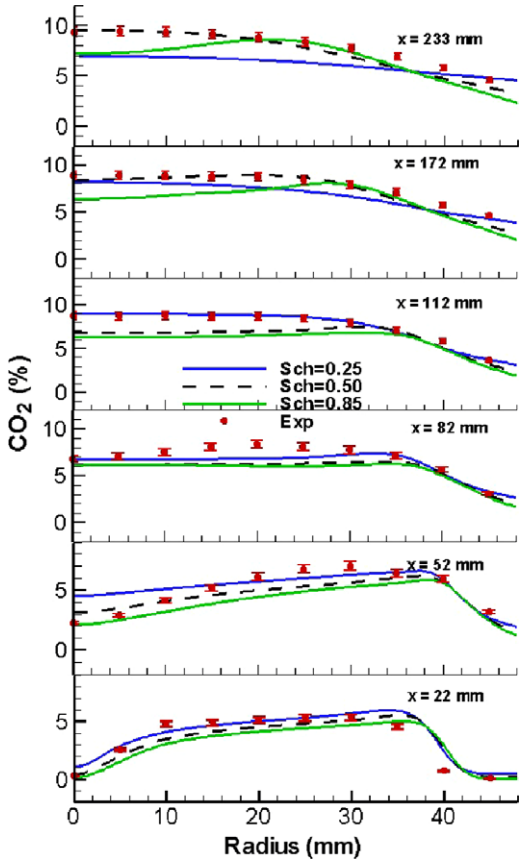

Fig. 17. CO_2 profiles at cross-sections, $x = 22$–233 mm.

measurements at two downstream sections ($x = 172$ and 233 mm) and one upstream section ($x = 52$ mm).

Carbon dioxide is another major product in propane–air combustion, while carbon monoxide is a major intermediate species. The predicted results are presented and compared with the measurements in Figs. 17 and 18, respectively. The experimental error bars of 5% are also included in these figures. As for the H_2O profiles in Fig. 16, the predicted species profiles show less variations along the radial direction as Γ_t decreases, particularly in downstream sections. The effect of Γ_t is significant at downstream sections and in some local regions at upstream sections. The predicted results with $\Gamma_t = 0.50$ show close agreement with the experimental database, except for section $x = 112$ mm.

At section $x = 112$ mm for $\Gamma_t = 0.50$, although the concentration of CO is over-predicted and that of CO_2 is under-predicted, the sum of the predicted CO and CO_2 agrees well with the sum of the measurements. This indicates a delay in CO oxidization prediction at this section. The results from $\Gamma_t = 0.85$ and 0.25 show large discrepancies from the measurements at downstream sections as well as in some local regions at upstream sections, particularly for the CO profiles.

Finally, it should be mentioned that in order to thoroughly assess the Reynolds analogy issue, numerical simulations were also carried out with the eddy-dissipation (EDS) and probability density function (PDF) combustion models. A large amount of numerical results and figures were generated. The trends and magnitudes of velocity, temperature and species distributions are similar to those obtained from the flamelet combustion model [32]. Although the results are not presented in this paper, the optimized Γ_t numbers are given in Table 1 for the purpose of comparison. During optimization, Γ_t number gradually decreased from 0.85 to 0.25 with an interval of 0.1 in general. Near the optimal value, an interval of 0.05 or even 0.01 was used. For temperature and species prediction inside the combustor, the numerical results were compared with and judged by the same experimental datasets, including velocity, temperature and species distributions. For wall temperature prediction, the optimal Γ_t number was judged mainly by the experimental temperature profile along the combustor wall.

As shown in Table 1, the optimal Γ_t for the temperature and species prediction inside the combustion chamber (line 1) is the same for all three combustion models; however, it (line 2) is different for the wall temperature prediction. This indicates that the combustion model has some effect on the near-wall temperature distribution.

4.4. Discussion

As shown in the above results, the optimal Γ_t number for the temperature and species prediction inside the

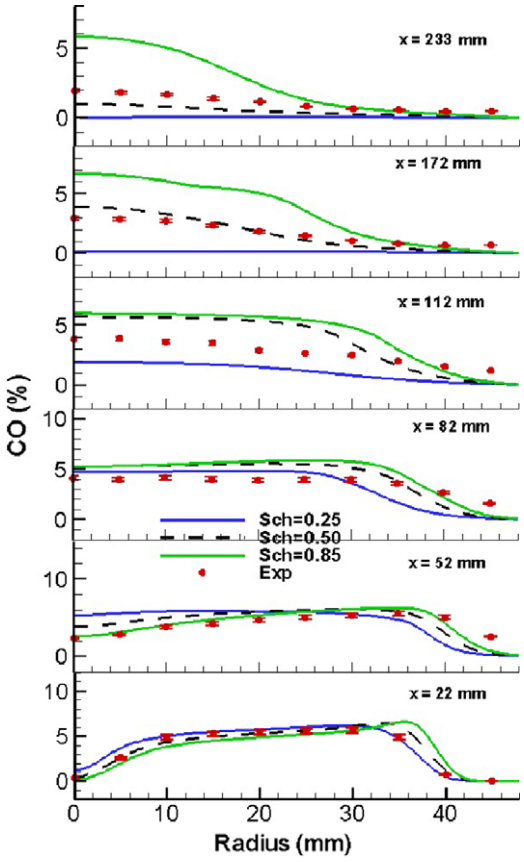

Fig. 18. CO profiles at cross-sections, $x = 22$–233 mm.

Table 1
Optimal Prandtl and Schmidt number

	Flamelet	PDF	EDS
T-chamber	0.50	0.50	0.50
T-wall	0.40	0.55	0.5–0.55

combustor is 0.50 for all three combustion models. This number is different from 0.25 in [17], 0.20 in [18] for kerosene-fired gas turbine combustors, and 0.20 for a cross-jet flow simulation [20]. However, it is the same as in [19] for a Rolls–Royce gas turbine combustor LES study.

All these examples reveal two important facts. First, the optimized value of Γ_t is lower than the traditionally used value of ~0.85. Second, the optimal value of Γ_t is most likely dependent on the combustor configuration and possibly the operating conditions. That is, a priori optimization of Γ_t is required in order to reasonably predict temperature and species distributions inside combustors. Obviously, this type of prior optimization is not practical in the real world.

The reasons for the above observations may be threefold. First, theoretically, Eqs. (8)–(10) are only valid for boundary layer flows, where the streamwise pressure gradient and source terms can be neglected. Certainly, its application to complex turbulent reacting flows is questionable. As stated earlier, a number of authors [7–10] have experimentally found that this analogy cannot apply to disturbed turbulent thermal boundary flows.

Second, the experimental values of Γ_t (~0.7) are obtained from fully developed boundary or pipe flows [2,3,12], and they may not be suitable for practical turbulent reacting flows. Therefore, in the sense of the average relative strength between the turbulence momentum and scalar transfers, a low value of Γ_t is a true fact and it may vary with flow configurations.

Third, Eqs. (8)–(10) are based on the gradient-type diffusion assumption which has been questioned by a number of researchers, particularly for turbulent energy and heat transfer [2]. Hinze [2] points out that both the gradient-type diffusion caused by small-scale turbulence and the convective action of large-scale turbulent motion should be considered in turbulent scalar transportations. It may be expected that the gradient-type diffusion approach is suitable for turbulent boundary flows; however, it is not suitable for complex flow fields inside combustion systems.

In summary, although the Reynolds analogy concept has been extended to flow field simulations since the 1970s, for accurate prediction of scalar transfers in turbulent reacting flows without prior optimization, this concept should be improved and new approaches should be developed. It is authors' wish that the outcome of this work could stimulate R&D activities on turbulence scalar transfers in numerical communities, and eventually solve industrial problems, such as temperature pattern factors at the exit of gas turbine combustors.

5. Conclusions

The effect of turbulent Prandtl/Schmidt number on the flow field of a propane diffusion flame combustor with the interior and exterior conjugate heat transfers has been numerically studied. Presented and discussed in this paper are some of the results obtained from a laminar flamelet combustion model with turbulent Prandtl/Schmidt number varying from 0.85 to 0.25. For completeness, the optimized Γ_t numbers for other two popular combustion models (EDS and PDF) are also provided.

In comparison with the comprehensive experimental database, it is found that the Γ_t number has limited effect on the velocity field. In contrast, it shows a strong effect on the temperature and species fields, particularly downstream in the combustor. This is also true for the temperature profile along the combustor wall.

For the present combustor configuration and operating conditions, the optimal Γ_t for temperature and species prediction inside the combustor is 0.5 for all three combustion models, and it varies from 0.40 to 0.55 for the combustor wall temperature prediction. With $\Gamma_t = 0.50$, the velocity, temperature and major species fields are reasonably well predicted, except in some local regions.

Finally, the rationale and limitation of the Reynolds analogy are discussed. For reliable temperature and species prediction in turbulent reacting flows without tuning

turbulent Pr_t and Sc_t numbers, the Reynolds analogy concept should be improved and new approaches should be studied.

Acknowledgements

The authors are grateful to Dr. Bill Wallace for his valuable comments and suggestions during the preparation of this paper. Also the authors want to express many thanks to Miss Abdelmesih Gewana (co-op student) for her assistance in the post-processing of numerical and experimental results.

References

[1] O. Reynolds, On the extent and action of the heating surface for steam boilers, Manchester Lit. Phil. 14 (1874) 7–12.
[2] J.O. Hinze, Turbulence, McGraw-Hill Book Company Inc., NY, 1987, pp.372–753.
[3] F.M. White, Heat and Mass Transfer, Addison-Wesley Publishing Company, NY, 1988, pp. 320–641.
[4] M.V. Suraweera, D.J. Mee, R.J. Stalker, Reynolds analogy in high-enthalpy and high-Mach-number turbulent flows, AIAA J. 44 (4) (2006) 917–919.
[5] J. Bons, A critical assessment of Reynolds analogy for turbine flows, Trans. ASME, J. Heat Transfer 127 (2005) 472–485.
[6] T.V. Jones, T.W. Walton, Reynolds analogy in film cooling, in: Tenth International Symposium on Air Breathing Engines, Nottingham, England, 1991, pp. 1263–1268.
[7] K.S. Choi, D.M. Orchard, Turbulence management using riblets for heat and momentum transfer, Exp. Therm. Fluid Sci. 15 (1997) 109–124.
[8] F. de Souza, J. Delville, J. Lewalle, J.P. Bonnet, Larger-scale coherent structures in a turbulent boundary layer interacting with a cylinder wake, Exp. Therm. Fluid Sci. 19 (1999) 204–213.
[9] J.C. Vogel, L.K. Eaton, Combined heat transfer and fluid dynamic measurements downstream of a backward-facing step, J. Heat Transfer 107 (1985) 922–929.
[10] E.D. John, J.O. Keller, Time-resolved gas temperature in the oscillating turbulent flow of a pulse combustor pipe, Combust. Flame 80 (1990) 358–370.
[11] P.A. Libby, F.A. Williams, Fundamental aspects and a review, in: P.A. Libby, F.A. Williams (Eds.), Turbulent Reacting Flows, Academic Press, NY, 1994, pp. 1–61.
[12] N.R. Panchapakesan, J.L. Lumley, Turbulence measurements in axisymmetric jets of air and helium, part 2, helium jet, J. Fluid Mech. 246 (1993) 225–247.
[13] C.L. Lubbers, G. Brethouwer, B.J. Boersma, Simulation of the mixing of a passive scalar in a round turbulent jet, Fluid Dyn. Res. 28 (2001) 189–208.
[14] D.B. Spalding, Concentration fluctuations in a round turbulent free jet, Chem. Eng. Sci. 26 (1971) 95–107.
[15] X.S. Bai, L. Fuchs, Sensitivity study of turbulent reacting flow modeling in gas turbine combustors, AIAA J. 33 (10) (1995) 1857–1864.
[16] M.K. Lai, CFD analysis of liquid spray combustion in a gas turbine combustor, The IGTI Expo, Orlando, FL, 1997, 1997-GT-309.
[17] D.S. Crocker, D. Nickolaus, C.E. Smith, CFD modeling of a gas turbine combustor from compressor exit to turbine inlet, The IGTI Expo 1998, Stockholm, Sweden, 1998, 1998-GT-184.
[18] H. Kaaling, R. Ryden, Y. Bouchie, D. Ansart, P. Magre, C. Guin, RQL combustor development including design, CFD calculations, CARS measurements and combustion tests, in: Thirteenth International Symposium Air Breathing Engines, Chattanooga, TN, USA, 1997, ISABE 97-70697.
[19] S.M. Cannon, C.E. Smith, M.S. Anand, LES predictions of combustor emissions in an aero gas turbine engine, in: Thirty-ninth AIAA/ASME/SAE/ASEE Joint Propulsion Conference and Exhibit, Huntsville, Alabama, USA, 2003, AIAA-2003-4521.
[20] G. He, Y. Guo, A.T. Hsu, The effect of Schmidt number on turbulent scalar mixing in a jet-in-crossing flow, Int. J. Heat Mass Transfer 42 (1999) 3727–3738.
[21] I. Campbell, D.L. Logan, An experimental study of a combusting flow past a confined bluff body, Combustion Institute – Canadian Section, Halifax, Canada, 1997.
[22] J.H. Ferziger, M. Peric, Computational Methods for Fluid Dynamics, Springer-Verlag, NY, 2002, pp. 1–10.
[23] Fluent Inc., Fluent 6.2 Documentation, 10 Cavendish Court, Lebanon, NH 03766, USA, 2006.
[24] L.Y. Jiang, I. Campbell, Turbulence modeling in a model combustor, Can. Aeronaut. Space. J. 53 (2) (2007) 45–57.
[25] B.E. Launder, G.J. Reece, W. Rodi, Progress in the development of a Reynolds-stress turbulence closure, J. Fluid Mech. 68 (1975) 537–566.
[26] N. Peters, Laminar diffusion flamelet models in non-premixed turbulent combustion, Prog. Energy Combust. Sci. 10 (1984) 319–339.
[27] K.N.C. Bray, N. Peters, Laminar flamelets in turbulent flame, in: P.A. Libby, F.A. Williams (Eds.), Turbulent Reacting Flows, Academic Press, NY, 1994, pp. 609–638.
[28] G. Stahl, J. Warnatz, Numerical investigation of time-dependent properties and extinction of strained methane- and propane–air flamelets, Combust. Flame 85 (1991) 285–299.
[29] G.D. Raithby, E.H. Chui, A finite-volume method for predicting a radiant heat transfer in enclosures with participating media, J. Heat Transfer 112 (1990) 415–423.
[30] NIST, NIST-JANAF Thermochemical Tables, fourth ed., Washington DC, 1998.
[31] J.P. Sislian, L.Y. Jiang, R.A. Cusworth, Laser Doppler velocimetry investigation of the turbulence structure of axisymmetric diffusion flames, Prog. Energy Combust. Sci. 14 (2) (1988) 99–146.
[32] L.Y. Jiang, I. Campbell, Prandtl/Schmidt number effect on temperature distribution in a generic combustor, in: The XVIII International Symposium Air Breathing Engine Conference, ISABE-2007-0178, September 2–7, 2007, Beijing, China.